AD_____

Award Number: W81XWH-11-1-0246

TITLE: Targeted Silver Nanoparticles for Dual-Energy Breast X-Ray Imaging

PRINCIPAL INVESTIGATOR: Andrew D. A. Maidment, Ph.D.

CONTRACTING ORGANIZATION: University of Pennsylvania
                          Philadelphia, Pennsylvania 19104

REPORT DATE: Maã´å 2013

TYPE OF REPORT: Final

PREPARED FOR: U.S. Army Medical Research and Materiel Command
               Fort Detrick, Maryland 21702-5012

DISTRIBUTION STATEMENT: Approved for public release;
                        distribution unlimited

The views, opinions and/or findings contained in this report are those of the author(s) and should not be construed as an official Department of the Army position, policy or decision unless so designated by other documentation.

REPORT DOCUMENTATION PAGE

Public reporting burden for this collection of information is estimated to average 1 hour per response, including the time for reviewing instructions, searching existing data sources, gathering and maintaining the data needed, and completing and reviewing this collection of information. Send comments regarding this burden estimate or any other aspect of this collection of information, including suggestions for reducing this burden to Washington Headquarters Services, Directorate for Information Operations and Reports, 1215 Jefferson Davis Highway, Suite 1204, Arlington, VA 22202-4302, and to the Office of Management and Budget, Paperwork Reduction Project (0704-0188), Washington, DC 20503

1. Agency Use Only (Leave blank)	2. Report Date Ráã´å 2013	3. Report Type and Period Covered (i.e., annual 1 Jun 00 - 31 May 01) Final (1 Ráã´å 201F – GÎ Ôæâã|áã] 2013)

4. Title and Subtitle Targeted Silver Nanoparticles for Dual-Energy Breast X-Ray Imaging	5. Award Number W81XWH-11-1-0246

6. Author(s)
Andrew D. A. Maidment, Ph.D.

7. Performing Organization Name (Include Name, City, State, Zip Code and Email for Principal Investigator) University of Pennsylvania Philadelphia, PA 19104 E-Mail: Andrew.Maidment@uphs.upenn.edu	8. Performing Organization Report Number (Leave Blank)

9. Sponsoring/Monitoring Agency Name and Address U.S. Army Medical Research and Materiel Command Fort Detrick, Maryland 21702-5012	10. Sponsoring/Monitoring Agency Report Number (Leave Blank)

11. Supplementary Notes (i.e., report contains color photos, report contains appendix in non-print form, etc.)

12a. Distribution/Availability Statement (check one) Approved for public release; distribution unlimited	12b. Distribution Code (Leave Blank)

13. Abstract *(Maximum 200 Words)* *(abstract should contain no proprietary or confidential information)*

We proposed to develop a silver (Ag) nanoparticle (NP) contrast agent optimized for dual-energy (DE) contrast-enhanced (CE) breast x-ray imaging. CE digital breast imaging provides an accurate method for decomposition of images into distinct breast tissue and contrast agent signals. At present, DE-CE breast imaging is performed with an iodinated contrast agent better suited for temporal subtraction CE imaging. We postulated that AgNP would be a superior contrast agent for DE-CE breast x-ray imaging. Ag filters can be used in the low-energy image acquisition to obtain a spectrum weighted just below the k-edge of Ag (25.5 keV). A low-energy spectrum optimized for Ag would also provide a superior anatomical image. We have demonstrated in proof-of-principle, the applicability of AgNP as contrast agents for use in DE-CE digital breast tomosynthesis and digital mammography. Three objectives have been met: 1) Synthesize and functionalize AgNP that are monodisperse in shape, size and distribution; 2) Perform vascular-enhancement, biodistribution and toxicity studies on mice; and 3) develop optimal x-ray imaging techniques.

14. Subject Terms (keywords previously assigned to proposal abstract or terms which apply to this award) Breast Cancer, X-ray contrast agent, Gold Nanoparticles, Silver Nanoparticles	15. Number of Pages (count all pages including appendices) 40
	16. Price Code

17. Security Classification of Report Unclassified	18. Security Classification of this Page Unclassified	19. Security Classification of Abstract Unclassified	20. Limitation of Abstract Unlimited

NSN 7540-01-280-5500

Standard Form 298 (Rev. 2-89)
Prescribed by ANSI Std. Z39-18
298-102

FOREWORD

Opinions, interpretations, conclusions and recommendations are those of the author and are not necessarily endorsed by the U.S. Army.

N/A Where copyrighted material is quoted, permission has been obtained to use such material.

N/A Where material from documents designated for limited distribution is quoted, permission has been obtained to use the material.

N/A Citations of commercial organizations and trade names in this report do not constitute an official Department of Army endorsement or approval of the products or services of these organizations.

N/A In conducting research using animals, the investigator(s) adhered to the "Guide for the Care and Use of Laboratory Animals," prepared by the Committee on Care and use of Laboratory Animals of the Institute of Laboratory Resources, national Research Council (NIH Publication No. 86-23, Revised 1985).

 X For the protection of human subjects, the investigator(s) adhered to policies of applicable Federal Law 45 CFR 46.

N/A In conducting research utilizing recombinant DNA technology, the investigator(s) adhered to current guidelines promulgated by the National Institutes of Health.

N/A In the conduct of research utilizing recombinant DNA, the investigator(s) adhered to the NIH Guidelines for Research Involving Recombinant DNA Molecules.

N/A In the conduct of research involving hazardous organisms, the investigator(s) adhered to the CDC-NIH Guide for Biosafety in Microbiological and Biomedical Laboratories.

_____ 9/09/13
          PI - Signature   Date

Table of Contents

1) Introduction

Contrast-enhanced (CE) dual-energy (DE) x-ray imaging provides a technique to increase the contrast of radiographic imaging agents by suppressing the variation in signal between various tissue types. In the breast, this involves the suppression of the signal variation that results from differences in soft-tissue (adipose and glandular) composition across the image. By reducing the effect of the soft-tissue contrast, it is then possible to segment and quantify the signal from the exogenous imaging agent more accurately. Clinically, CEDE imaging is garnering significant interest because a) it is possible to obtain multiple views of both breasts with a single contrast administration; b) the contrast agent can be administered when the breast is uncompressed thus preserving the natural circulatory dynamics of the breast tissue; c) the high- and low- energy images can be obtained in quick succession, reducing patient motion.

At present, CEDE breast imaging is performed with iodinated contrast agents which are better suited for temporal subtraction CE imaging. We postulated that silver (Ag) nanoparticles (NP) would be superior as a contrast agent for CEDE breast x-ray imaging. Calculations of contrast as a function of two mono-energetic spectra showed that Ag is able to provide higher DE contrast than iodine. In parallel work, we have successfully fabricated AgNP which are stable and have yielded high-quality images. Here, we detail the results of our work. We have presented and published our results in conference proceedings. We have filed a provisional patent application. The main participant of the project, Roshan Karunamuni, is in the final months of his PhD, and his thesis, together with three peer-reviewed manuscripts are in preparation.

2) Keywords:

Breast Cancer, contrast-enhanced imaging, digital breast tomosynthesis, dynamic imaging, x-ray imaging

3) Overall Project Summary

a) Research Overview

In this grant, we postulated that AgNP would be superior as a contrast agent for CEDE breast x-ray imaging. We proposed to demonstrate in proof-of-principle, the applicability of AgNP as contrast agents for use in narrow-bandwidth CEDE-breast x-ray imaging. Two objectives were proposed:

> **O1**: Synthesize spherical AgNP and functionalize them with an anti-HER2/neu affibody.

> **O2**: Perform *in vitro* cytotoxicity, and *in vivo* tumor enhancement imaging and biodistribution studies.

We have successfully completed O1 and O2.

The results are divided into two major subsections:

a. Imaging Framework: In order to better understand the suitability of silver as a contrast agent, we expanded upon our primary calculations of contrast sensitivity. Simulations were performed using both monoenergetic and polyenergetic x-ray spectra to determine if silver is a viable alternative to iodine, as well as determine the set of imaging parameters needed to maximize the contrast. We have also tested our imaging method on physical phantoms.

b. Development of the silver contrast agent: We have also completed the synthesis and characterization of a silver nanoparticle-based contrast agent. The particles were then injected into immunocompromised mice which resulted in significant enhancement in the primary blood vessels, liver, and spleen.

We have excellent progress on this project and have presented these results at the 11th International Workshop in Breast Imaging 2012 and 2013 SPIE Physics of Medical Imaging. (see Appendix)

b) Results

i) Imaging Framework

The DE signal intensity (SI^{DE}) can be expressed as a logarithmic-weighted subtraction between the high- and low- energy signal intensities. By using the Beer-Lambert law, these intensities can be expressed as a combination of the linear attenuation coefficients (μ) and thicknesses (t) of the various materials in the beam path. Thus, SI^{DE} can be expressed as:

$$SI^{DE} = \ln(I_0^H) - W \times \ln(I_0^H) + t \times [-\mu_a^H + W \times \mu_a^L] + t_g \times [(\mu_a^H - \mu_g^H) - W \times (\mu_a^L - \mu_g^L) +$$

$$t_c \times [-\mu_c^H + W \times \mu_c^L] \qquad (1)$$

In Equation 1, the superscripts L and H refer to low- and high- energy respectively. The subscripts a, g, and c refer to adipose, glandular and contrast material respectively. I_0 is the initial photon fluence, μ is the linear attenuation coefficient, t is the thickness of the material, and W is the weighting factor.

SI^{DE} can be broken down into three major components. The first component, underlined in blue, is a combination of the initial photon fluence and total thickness of the breast. This component can be assumed to be constant across the image and thus provides an offset to SI^{DE}. The second component, underlined in red, states the relationship between SI^{DE} and the amount of glandular tissue in the beam. By choosing W as:

$$W = \frac{\mu_a^H - \mu_g^H}{\mu_a^L - \mu_g^L}, \qquad (2)$$

we can eliminate this dependence. Thus the only remaining term that varies across the image is the third component which is underlined in green. This component quantifies the linear relationship between SI^{DE} and the thickness of contrast material with a slope, S_C:

$$\frac{d(SI^{DE})}{d(t)} = S_C = -\mu_c^H + \frac{\mu_a^H - \mu_g^H}{\mu_a^L - \mu_g^L} \times \mu_c^L \qquad (3)$$

The noise (σ_{bkg}) in the background signal can be obtained from Equation 1, and formulated as

$$\sigma_{bkg} = \sqrt{\frac{1}{I_0^H e^{-\mu_a^H t_T}} + \frac{W^2}{I_0^L e^{-\mu_a^L t_T}}}, \qquad (4)$$

A total dose of 1.0 mGy was assumed for the LE and HE images, at a thickness of 5 cm. The dose distribution between the LE and HE images was however, allowed to vary. From Equations 11 and 12, the contrast-to-noise ratio (CNR) is calculated as:

$$CNR = \frac{S_C}{\sigma_{bkg}}.$$

W (see Figure 1) and S_C (see Figure 2) were calculated for energy combinations between 20 and 50 keV. W was found to have values ranging between 0 and 1 – this is to be expected as the difference in mass attenuation coefficients of adipose and glandular tissue decreases as the

7

energy increases. W tends towards 1 along the diagonal of the plot, for the case where the low and high energy are equal, and is smallest when the low- and high- energies are furthest apart.
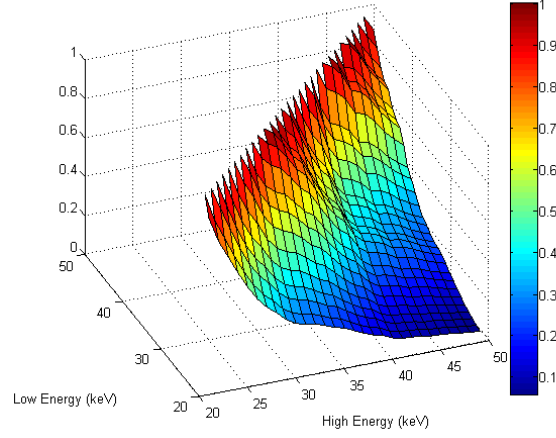

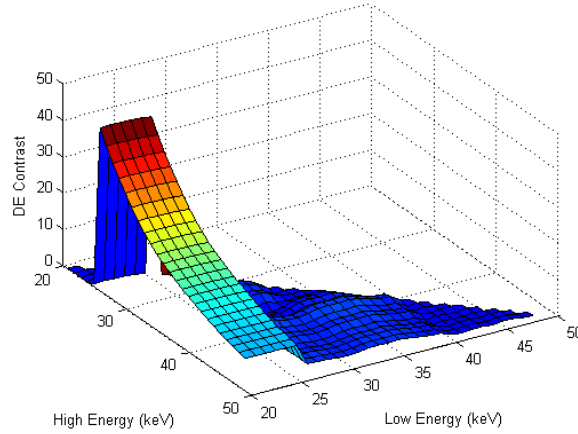**Figure 1.** W calculated for energy pairs between 20 and 50 keV. Values of W ranged from 0 to 1.

Figure 2. S_C for Silver calculated for energy pairs between 20 and 50 keV. The maximum contrast of 45 a.u. occurs at a low energy of 21 keV, and a high energy of 26 keV.

As expected, contrast is only observed with silver for energy pairs that bracket the k. The maximum contrast for silver is 45 a.u. and occurs at a low energy of 21 keV, and a high energy of 26 keV. Using the same method, the maximum contrast calculated for iodine was 28 a.u., indicating that silver can theoretically provide 1.5 times that the contrast of iodine in CEDE breast imaging.

The dependence of *CNR* on energy and material is demonstrated in Figure 3. The graphs are plotted for a thickness of 5 cm, with a dose fraction of 0.5 to the LE image. Similar to S_C, a large value of *CNR* is only obtained for energy pairs that bracket the k-edge of the material. *CNR* is not observed for materials, such as Au, whose k-edge lies outside of the energy range. However, the variation in *CNR* is less than that of S_C. For example the maximum S_C for Ag is 1.6 times that

of iodine, whereas the maximum *CNR* at a dose fraction of 50% is 1.04 times that of iodine. This discrepancy between the trend in S_C and *CNR* is a result of the noise. The noise increases substantially for lower energies because of the poor penetration through the breast resulting in fewer x-rays being detected. This penalizes materials with lower atomic numbers, and consequently lower k-edges
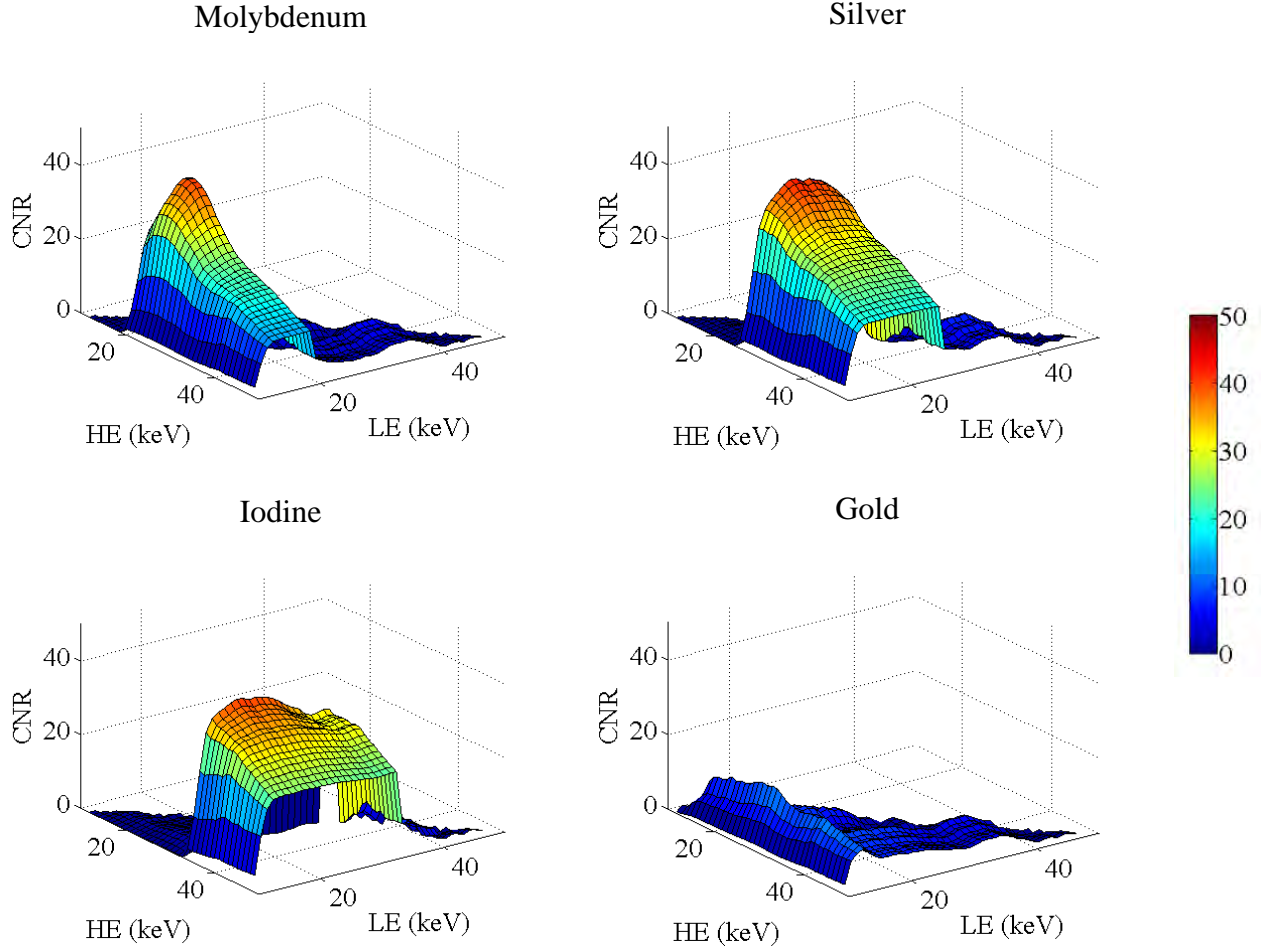

Figure 3. Energy dependence of *CNR* for molybdenum, silver, iodine, and gold for a dose distribution of 50% to LE. Similar to S_C, *CNR* is only observed for energy pairs that bracket the k-edge of the material. The choice of contrast material does not have as large an impact on the maximum achievable *CNR* as it does on S_C. The *CNR* for Au is, however, much lower than the other materials at this dose distribution.

The maximum *CNR* for every material in the range of Z = 1 to 80 is shown in Figure 4. The corresponding dose fractions that result in these optimal points is overlaid. The graph can be divided into two main regions: R1) atomic numbers less than 33 or greater than 63, and R2) atomic numbers between 34 and 62. The materials in R1 exhibit very little contrast due to the absence of a k-edge in the energy range studied. The dose fraction in this range assumes values between 0.1 and 0.5 in an effort to reduce the noise. The more interesting effects are observed in R2. The *CNR* slowly increases and reaches a plateau between materials with atomic numbers from 42 to 63. Within this plateau, the maximum *CNR* differs by less than 15%. The absolute

maximum occurs at Z = 59, Praseodymium, with a dose fraction of 0.2 to the LE at an (LE, HE) energy pair of (18,42). The dose fraction within R2 reaches its maximum value of 0.7 at an atomic number of 34. As the atomic number increases, the optimal dose fraction decreases until it reaches its minimum value of 0.1 at an atomic number of 63.
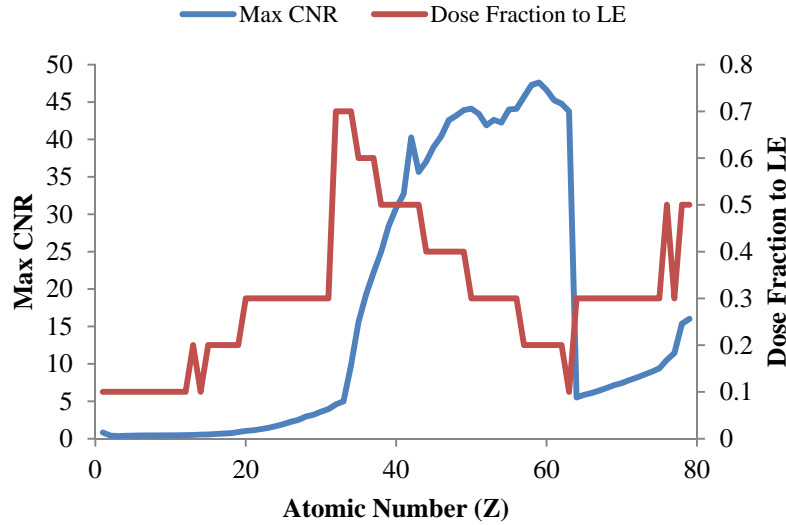

Figure 4. Overlay of the maximum *CNR* and corresponding dose distribution for materials with Z ranging from 1 to 80. There exists a group of materials from Z = 42 to 63, where the maximum *CNR* does not change by more than 15%. This group of materials represent the optimum selection for contrast agents in CEDE breast imaging.

Among the materials with the optimal group of materials, silver lies in an optimal position for CEDE imaging. As Z increases within this group, the optimal HE value increases while the optimal dose fraction to the LE decreases. In order to obtain a HE spectrum with a high mean energy value, large amounts of filtration will have to be added into the beam. This requires a sometimes unfeasible tube current to ensure enough photon fluence reaches the detector. In addition, a low dose fraction to the LE image will result in noisier anatomical images that will limit the effectiveness and applications of the imaging technique. Therefore, when considering both of these constraints, materials with low *Z* (such as silver) in the plateau group are preferred.

A spectral simulation search was performed to identify the combination of clinically-feasible imaging parameters that maximized signal difference to noise ratio (*SDNR*) for Ag. The parameters chosen for the search are shown in Table 1**Error! Reference source not found.**. These parameters reflect those that are available on the Hologic clinical contrast-enhanced dual-energy image acquisition system.

Table 1. Values of parameters used in the simulation algorithm

Parameter	Values
Target	Tungsten
Low Energy kVp	23 to 35
High Energy kVp	36 to 49
Filter Materials	Low Energy: Ag, Rh, Al
	High Energy: Cu
	All spectra were pre-filtered with air and beryllium
Detector	Si, energy-integrating, 200 µm
Breast Thickness	2 to 8 cm

In total, 26,460 combinations of imaging parameters were studied. Polyenergetic tungsten spectra were simulated using Boone's interpolation methods [1] and filtered using the Beer-Lambert law. A low- and high- energy spectral pair were then passed through 5 cm of 100% adipose or glandular tissue. W can be calculated using signal intensities (SI) as:

$$W = \frac{SI_a^H - SI_g^H}{SI_a^L - SI_g^L} \qquad (3)$$

Experimental and simulated values of W were compared to determine if the simulation algorithm is able to accurately predict the signal intensities recorded by the image acquisition system. The results are shown in Figure 5, with a Pearson correlation coefficient of 0.96 between the two data sets, suggesting an excellent correlation.

The dual-energy signal intensity (SI^{DE}) is calculated from the low(L)- and high(H)-energy (E) signal intensity as:

$$SI^{DE} = SI^{HE} - W \times SI^{LE}$$

The calculation is performed for breast tissue with (subscript: *cont*) and without (subscript: *bkg*) added contrast material. The resulting image contrast is quantified using the signal difference to noise ratio (*SDNR*) as:

$$SDNR = \frac{SI_{cont}^{DE} - SI_{bkg}^{DE}}{\sigma_{bkg}^{DE}}$$

The standard deviation in the dual-energy signal intensity is calculated as:

$$\sigma^{DE} = \sqrt{\sigma^{2^H} + W^2 \times \sigma^{2^L} - 2 \times W \times cov(\ln(SI_{bkg}^H), \ln(SI_{bkg}^L))}$$

The experimentally obtained values of *SDNR* were compared to those obtained from the simulation algorithm and plotted in Figure 6. The two sets of data showed excellent correlation with a Pearson correlation coefficient of 0.93. This indicates that the simulation algorithm is able to correctly predict the trends in signal intensity observed in the Hologic Dimensions CEDE system.
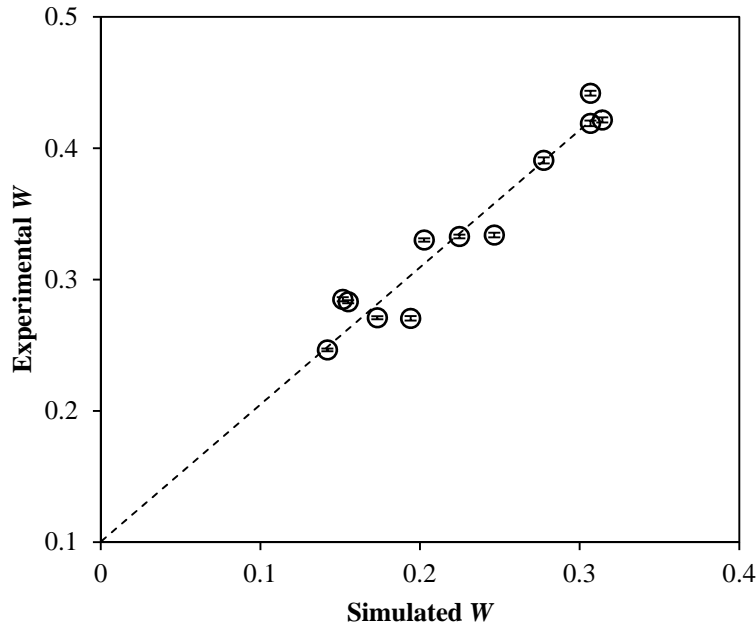

Figure 5. The experimentally-obtained values of *W* are highly correlated with the simulated values. A Pearson correlation coefficient of 0.96 was calculated for the two data sets. Error bars indicate standard deviation.
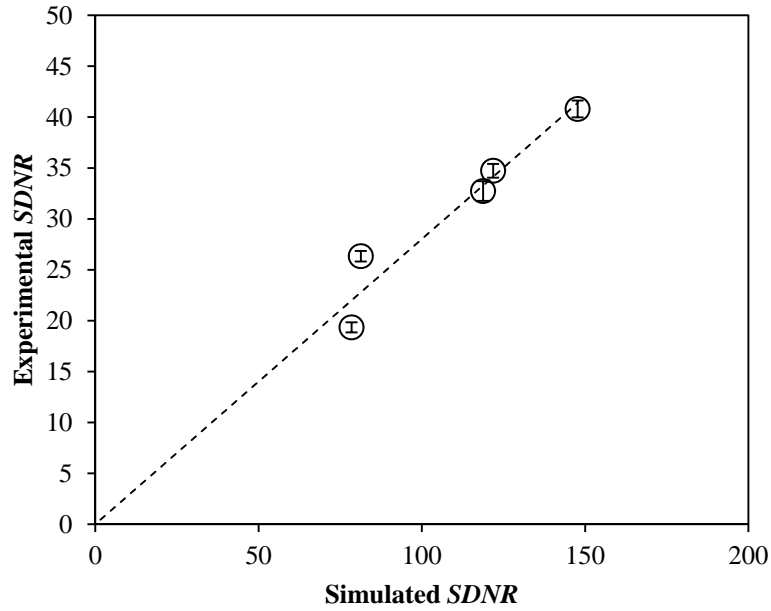
Figure 6. The experimentally-obtained values of *SDNR* correlate well with the simulated values. A Pearson correlation coefficient of 0.93 was obtained between the two data sets.

The optimal imaging parameter conditions for breast thicknesses ranging from 2 to 8 cm using a silver contrast agent are tabulated in Table 2. The LE kVp is maintained at 26 kVp while the HE kVp and dose distribution to the LE are steadily increased for increasing breast thickness. A Rh filter is selected throughout the thickness range except for the largest breast, where Ag filtration is preferred. The LE image, consisting of a 26 KVp tungsten spectra filtered with Rh is a classic example of a soft-tissue anatomical image obtained clinically. Therefore, the LE image would provide excellent anatomical and spatial localization of structures, (calcifications, lesions), while the DE image can be used for quantitative analysis of contrast agent uptake.

Table 2. Optimal combinations of parameters to maximize *SDNR* of silver at breast thicknesses from 2 to 8 cm. The LE kVp is maintained at 26 kVp, while the HE kVp and dose distribution to the LE is increased as the breast thickness increases.

Breast Thickness (cm)	HE kVp	LE kVp	LE filter	Dose distribution to LE (%)
2	44	26	Rh	30
3	45	26	Rh	30
4	49	26	Rh	30
5	49	26	Rh	40
6	49	26	Rh	60
7	47	26	Rh	70
8	49	26	Ag	70

The simulation was then used to identify the spectral combinations that optimized the *SDNR* for an iodine contrast agent. 16 mg/mL of iodine or silver solution were then injected into a custom-built- step phantom, and imaged using the optimal conditions for iodine and silver. The technique parameters were grouped by filter material so that for each filter, four imaging conditions were carried out: (i) silver(Ag) at optimal silver, (ii) iodine (I) at optimal iodine, (iii) silver at optimal iodine, and (iv)iodine at optimal silver. The *SDNR* of the four conditions was measured and then plotted in Figure 7.
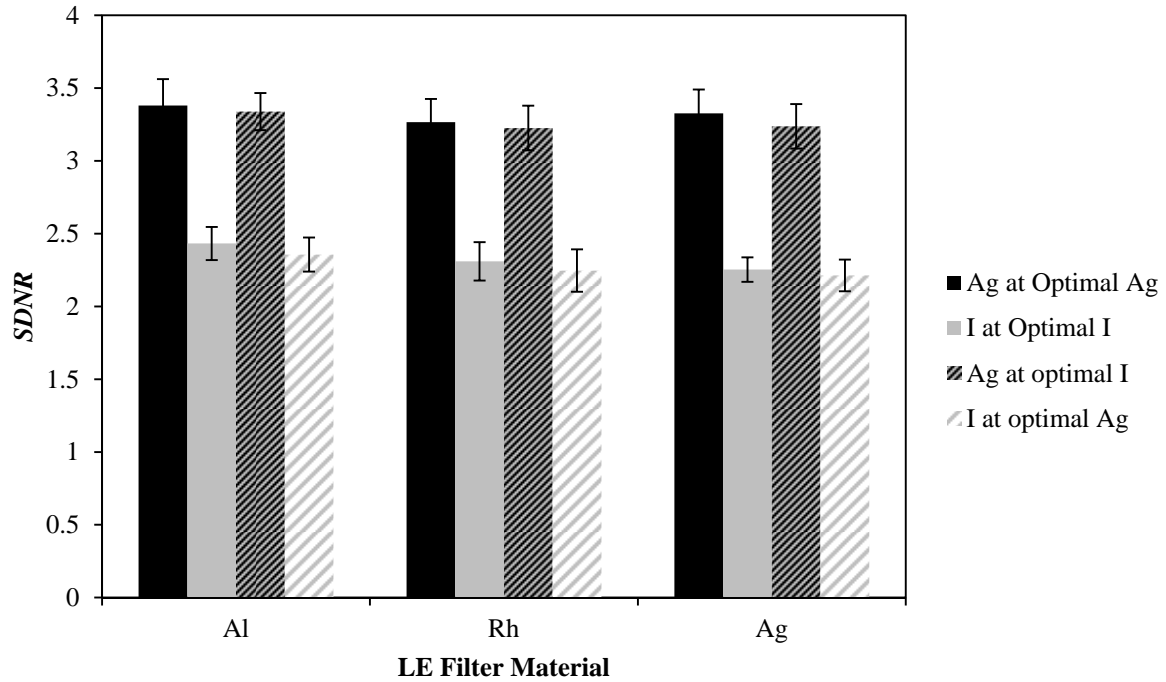
Figure 7. Comparison of *SDNR* between Ag and I for the optimal imaging parameters at each LE filter material. Ag performs better that Iodine at their respective optimal imaging conditions, regardless of the filter material. In addition, I imaged at the optimal conditions for I performs worse than Ag at those same conditions.

When imaged at their respective optimal conditions, Ag outperforms iodine regardless of the filter material chosen. On average, the *SDNR* for Ag is 43% higher than that of I. The superiority of Ag is such that the lowest *SDNR* for Ag is still 34% higher than the highest *SDNR* for I. The improved *SDNR* for Ag when compared to I can be attributed to the lower k-edge of Ag. When considering each material imaged at their respective optimal conditions, the lower k-edge of Ag means that the HE spectrum can be better positioned for optimal DE contrast. Theoretical analysis demonstrated that DE contrast is very sensitive to the placement of the HE value, specifically the contrast decreases rapidly as the HE value is further away from the k-edge of the contrast material. It is difficult to obtain HE spectra with mean energies in the range of 34 – 38 keV (above the k-edge of I) using clinically-reasonable amounts of filtration. It would require kVp values on the order of 50 – 60 kVp with moderate amounts of filtration or large amounts of filtration with a large portion of the dose allocated to the HE to accommodate the lower fluence. Therefore, Ag can be imaged at near optimal conditions on a clinical system while I must be imaged with sub-optimal imaging parameters.

In addition, Ag performs better than I when imaging at the optimal conditions for I. For example, using a rhodium filter, the *SDNR* for Ag is 40% higher than that of I at the optimal conditions for I. The maximum *SDNR* for I occurs at a HE kVp value of 49. This is needed to ensure that a large portion of the spectrum above the k-edge of I. However, even at the maximum kVp value, a

15

substantial portion of the HE spectrum is below the k-edge of I, and thus not contributing to the *SDNR*. When using a 49 kVp HE spectrum with the copper filter available on the Hologic CEDE system, 99% of the spectrum by number of photons is above the k-edge of Ag while only 78% is above the k-edge of I. The remaining 22% of the spectrum below the k-edge of I cannot contribute to the *SDNR* of I, providing Ag with an advantage, even at the best possible conditions for I.

ii) Development of AgNP agent

Concurrently, we have worked on the development of the silver nanoparticle imaging agent. An overview of the synthesis procedure is shown in Figure 8. Spherical silver (Ag) cores are first synthesized using methods provided by the literature. The cores are then encapsulated within a silica (Si) shell in an attempt to reduce the formation of toxic Ag^+ ions. The shell was designed so as to prevent the oxidation of the silver surface by biological components found in living systems. The entire silica-silver construct was entrapped in a polymeric micelle that possessed a polyethylene glycol outer layer to improve the biological compatibility of the nanoparticle system.

Synthesis of silver core: The silver core is synthesized as described by Silvert *et al.*[1]. Briefly, 1.5 g of polyvinylpyrrolidone (PVP) was dissolved in 75 mL of ethylene glycol in a 250 mL roundbottom flask fitted with a condensation apparatus and left overnight to complete mixing. 50 mg of silver nitrate ($AgNO_3$) was then added. The suspension was heated to 120 °C at a rate of 1 °C/minute. The reaction was allowed to proceed at this temperature for 1 hour. The mixture was then cooled to room temperature. The PVP-stabilized silver nanoparticles were purified by adding acetone to the reaction vessel and centrifuging at 4000 xg for 15 minutes. The particles were then resuspended in ethyl alcohol for further modification.

Silica encapsulation of silver core: The PVP-stabilized silver cores were then encapsulated within a silica shell using the method described by Graf *et al*. [2]. 416 µL of ammonium hydroxide was added to 9.438 mL of PVP-stabilized silver nanoparticles, after which 75 µL of tetraethoxysilane (TES) in 675 µL of ethyl alcohol is added. The reaction is then allowed to proceed in the dark for 12 hours. The silica-silver nanoparticles are then purified by centrifugation at 19,000 xg for 15 minutes, and resuspended in ethyl alcohol.

PEG-stabilization of silica-silver particles: The silica-silver nanoparticles were then individually incorporated into a polymeric micelle to ensure biocompatibility of the particles. This is a two-step process, in which the nanoparticles are first made lipophilic using the method described by Koole *et al.*[3]. The silica-silver nanoparticles were mixed with excess octadecanol in ethyl alcohol and heated to 100 °C for 1 hour to remove the ethanol. The mixture is then heated to 170 °C for 3 hours to covalently link the octadecanol to the silica-silver nanoparticles by a condensation reaction. The octadecanol-coated silica-silver nanoparticles were dispersed in toluene, and mixed with , an amphiphilic ligand that contains a lipophilic polycaprolactone chain

and a hydrophilic polyethylene glycol chain at a mass ratio of 1:4. The PEG-coated silica-silver nanoparticles (PEG-Si-AgNP) were then purified using centrifugal filtration to remove any unwanted byproducts and excess reagents.
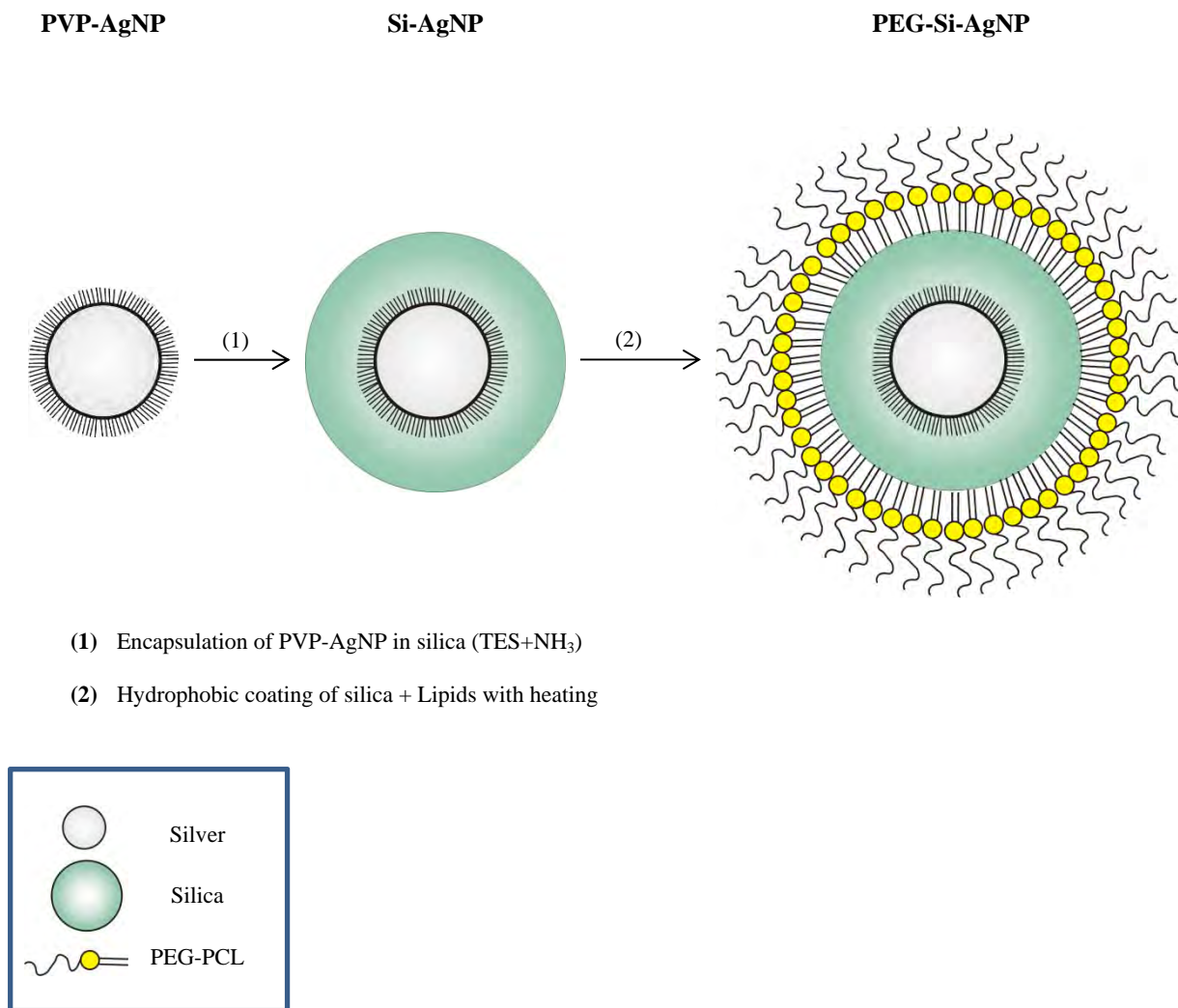
PVP-AgNP   **Si-AgNP**   **PEG-Si-AgNP**

(1)   Encapsulation of PVP-AgNP in silica (TES+NH$_3$)

(2)   Hydrophobic coating of silica + Lipids with heating

Figure 8. Schematic of the procedure to synthesize silver nanoparticle-based imaging agent. Silver cores are first synthesized, and then encapsulated within a silica shell. The shell is made hydrophobic, and then incorporated into a polymeric micelle to enhance the biocompatibility of the nanostructure.

Transmission electron microscopy (TEM) was used to image and calculate the diameter of the nanoparticles at each stage of the synthesis. The PVP-coated silver cores are shown in Figure 9. The particles consist of solid, spherical silver cores with an average diameter of 39 ± 6 nm (mean ± standard deviation). After silica encapsulation, the total diameter of the nanoparticles is 102 ± 9 nm (Figure 10). The majority of the silica-silver nanoparticles consisted of a single silver core covered by a spherical silica shell. The PEG-PCL layer of the final AgNP nanoparticle is electron-transparent and thus does not appear in the TEM micrograph (Figure 11). The particles

were, however, observed to be separated from each other indicating that a polymeric surface layer was successfully attached to each silica-silver nanoparticle.
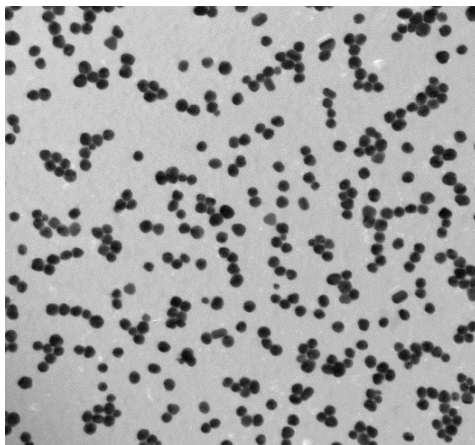

Figure 9. TEM image of PVP-coated silver nanoparticles. The nanoparticles are spherical with a solid silver core measuring 39 ± 6 nm.
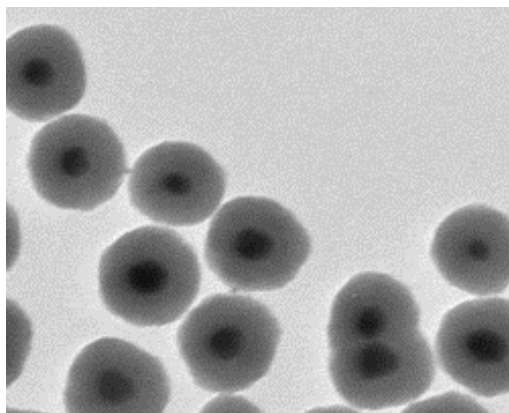

Figure 10. TEM image of Si-coated silver nanoparticles with an average diameter of 102 ± 9 nm. The majority of the particles consist of a single silver core encapsulated with a silica shell.
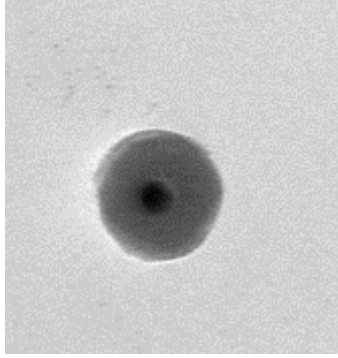
Figure 11. TEM image of AgNP. The PEG-PCL layer surrounding the silica-silver nanoparticles is electron-transparent and therefore does not appear in the image.

Immunocompromised mice were injected with 600 mg/kg of silica-silver nanoparticles. Immediately post-injection, the animals were imaged initially using a small animal, micro-CT scanner at 45 kVp. The images demonstrated significant enhancement in the heart, liver, and primary and peripheral blood vessels (Figure 2). The mice were re-imaged 24 hours after the injection, and the majority of the particles were located in the spleen and liver, with minimum enhancement observed in the heart and other organs.

Figure 12. :**Left:** Reconstructed slice of micro-CT volumetric data set obtained before injection of AgNP. **Middle:** Reconstructed slice obtained immediately post-injection of AgNP at a dose of 600 mg silver/kg of body weight. Significant contrast is observed immediately post-injection in both the heart and liver (yellow arrows). **Right:** False color image of volumetric data showing significant enhancement in peripheral and primary blood vessels.

4) Key Research Accomplishments

- Created a mono-energetic model of dual-energy x-ray imaging with silver contrast agents.
- Created a poly-energetic model of dual-energy x-ray imaging with silver contrast agents.
- Developing a subtraction method of silver imaging based on the attenuation properties of the material
- Identified a synthesis method for silver nanoparticles which is non-toxic
- Characterized the silver nanoparticles in terms of size (TEM and DLS)
- Injected si-encapsulated AgNP polymeric micelles into immunocompromised mice

5) Conclusions

This work explored the use of Ag imaging agent as an alternative to iodine in CEDE x-ray breast imaging. Iodinated agents are used extensively in x-ray projection imaging and display excellent biocompatibility and stability within the body. However, the lower energies available to clinical DE x-ray breast imaging compared to other organs in the body suggests that an alternative material may be better suited. Theoretical analysis demonstrated that materials with atomic numbers from 42 to 63 should be explored as potential candidates. From these materials, Ag was chosen for further investigation. The prominence of Ag filters in breast x-ray imaging devices and Ag nanoparticles in consumer products suggested that a Ag nanoparticle-based imaging agent could provide benefit in CEDE x-ray breast imaging. An algorithm was developed in MATLAB to simulate the image acquisition of the Hologic Dimensions CEDE system. The *SDNR* of Ag was compared to that of I for various imaging conditions that comprised of the optimal conditions for either material. Not only does Ag perform better than I when imaged at their respective optimal conditions, but Ag is able to provide greater contrast when imaged using protocols that are currently being used for I. This means that a Ag contrast agent could be translated to the clinic without modification of machine or protocol. Silver nanoparticles were successfully encapsulated with a silica shell and stabilized within a biocompatible polymeric micelle. The particles showed significant enhancement within the heart, liver, and primary blood vessels of immunocompromised mice. This work has led to three conference presentations, two conference papers, and a provisional patent application. It is anticipated that by the end of 2013, the graduate student working on this project will have completed his PhD and three peer-reviewed papers will be submitted.

6) Publications, Abstracts, and Presentations

Karunamuni, R., Zaki, A.A., Popov, A.V., Delikatny, E.J., Gavenonis, S., Tsourkas, A., Maidment A. "An examination of silver as a radiographic contrast agent in dual-energy breast x-ray imaging." LNCS; 785: 418-425, 2012

Karunamuni, R., Maidment, A. "Quantification of a silver contrast agent in dual-energy x-ray imaging." Proceedings of SPIE 8668, 2013

Roshan Karunamuni, Ajlan Al-Zaki, David Cormode, Anatoliy Popov, Jim Delikatny, Andrew Tsourkas, Andrew D.A. Maidment. "Silica-encapsulated silver nanoparticles as contrast agents for contrast-enhanced dual-energy x-ray breast imaging." 3rd Annual TMII Symposium, July 2013, New York, NY.

7) Inventions, Patents and Licenses

Provision Patent Application, Ref P-76220-USP1, RADIOGRAPHIC CONTRAST AGENTS FOR TEMPORAL SUBTRACTION AND DUAL-ENERGY X-RAY IMAGING, Roshan Karunamuni, Ajlan Al Zaki, Anatoliy V. Popov, E. James Delikatny, Sara Gavenonis, Andrew Tsourkas, Andrew D. A. Maidment.

8) Reportable Outcomes

N/A

9) Other Achievements

Roshan Karunamuni, Ph.D., Bioengineering, University of Pennsylvania, Dec 2013 (est.)

10) References

[1]   P. Silvert, N. Duvauchelle, V. Vijayakrishnan, and K. T. Elhsissen, "Preparation of colloidal silver dispersions by the polyol process," *Journal of material chemistry*, vol. 6, no. 4, pp. 573–577, 1996.

[2]   C. Graf, D. L. J. Vossen, A. Imhof, and A. van Blaaderen, "A General Method To Coat Colloidal Particles with Silica," *Langmuir*, vol. 19, no. 17, pp. 6693–6700, Aug. 2003.

[3]   R. Koole, M. M. van Schooneveld, J. Hilhorst, K. Castermans, D. P. Cormode, G. J. Strijkers, C. de Mello Donegá, D. Vanmaekelbergh, A. W. Griffioen, K. Nicolay, Z. a Fayad, A. Meijerink, and W. J. M. Mulder, "Paramagnetic lipid-coated silica nanoparticles with a fluorescent quantum dot core: a new contrast agent platform for multimodality imaging.," *Bioconjugate chemistry*, vol. 19, no. 12, pp. 2471–9, Dec. 2008.

11) Appendix

Karunamuni, R., Zaki, A.A., Popov, A.V., Delikatny, E.J., Gavenonis, S., Tsourkas, A., Maidment A. "An examination of silver as a radiographic contrast agent in dual-energy breast x-ray imaging." LNCS; 785: 418-425, 2012

Karunamuni, R., Maidment, A. "Quantification of a silver contrast agent in dual-energy x-ray imaging." Proceedings of SPIE 8668, 2013

An examination of silver as a radiographic contrast agent in dual-energy breast x-ray imaging

Roshan Karunamuni[1], Ajlan Al Zaki[2], Anatoliy V. Popov[1], E. James Delikatny[1], Sara Gavenonis[1], Andrew Tsourkas[2], Andrew D. A. Maidment[1].

[1]University of Pennsylvania, Department of Radiology, Philadelphia USA
[2]University of Pennsylvania, Department of Bioengineering, Philadelphia, USA
aros@seas.upenn.edu, andrew.maidment@uphs.upenn.edu

Abstract. Silver nanoaprticles have been investigated as an alternative to iodine in dual-energy breast x-ray imaging. Dual-energy imaging involves acquiring images at two distinct energy windows (low and high). Weighting factors are then applied to create an image where the contrast between background tissues has been suppressed. Silver (Ag) represents an attractive contrast material due to its favorable x-ray attenuation properties (k-edge of 25.5 keV). Theoretical analysis using polychromatic spectra shows that silver can provide similar, if not better, contrast to iodine. Spherical Ag nanoparticles with an average diameter of 4 ±2 nm were synthesized using the Brust method in water. The particles were surface stabilized with polyethylene glycol and showed little cellular toxicity in T6-17 fibroblast cells. These results have encouraged further investigation into validation and testing in living system models. Silver nanoparticles represent an exciting avenue for the development of a novel dual-energy, x-ray breast imaging agent.

1   Introduction:

Contrast-enhanced dual-energy (DE) x-ray imaging provides a technique to increase the contrast of radiographic imaging agents by suppressing the variation in signal between various tissue types. In the breast, this involves the suppression of the signal variation between admixtures of glandular and adipose tissue. By reducing the effect of this "anatomical noise", it is then possible to more accurately segment and quantify the signal from the contrast agent. Dual-energy imaging utilizes two distinct energy windows (low- and high-) to quantify the variation in attenuation with energy. To achieve a suitable contrast between imaging agent and tissue, it is therefore necessary that their respective attenuation profiles do not follow the same general trend from low- to high- energy. This can be done by using a contrast material whose k-edge lies between the two energy windows. The discrete jump in attenuation due to the photoelectric effect of the extra k-shell electrons means that the contrast material exhibits a markedly different attenuation profile to the surrounding tissue.

Currently, the majority of research that is performed in dual-energy x-ray imaging involves iodinated contrast agents. Silver (Ag) represents an attractive alternative due

to the location of its k-edge (25.5 keV) within the range of clinically-used mammographic energies. Silver filtration is also common in the clinical setting, which could provide additional benefit with a silver imaging agent. The aim of this study is to provide an experimental argument for Ag in breast DE x-ray imaging, and to develop a prototype Ag nanoagent for testing in living systems.

2   Results (Theoretical Simulations):

Monoenergetic analysis: A monoenergetic analysis was first performed to identify candidate combinations of low (LE) and high (HE) energies. Linear attenuation coefficients (LAC) were calculated for various admixtures of glandular and adipose tissues ranging from 0 to 100% glandular. Separately, the LAC were calculated for a 50% glandular, 50% adipose composite with increasing concentrations of contrast material. Mass attenuation coefficients needed for this calculation were obtained from the NIST XCOM online physics database [1]. Energy pairs ranging from 15 to 45 keV (in 1 keV intervals) were studied. For each energy-pair, two-dimensional maps of linear attenuation coefficients for tissue were calculated in terms of glandularity and concentration of silver (see Figure 1). Linear relationships were observed for both variables. The metric R was defined as the angular separation between these two linear fits.

An energy pair of (20, 30) keV was identified to maximize R (44°) using a silver contrast agent. A similar calculation for iodine showed that R was maximum at an energy pair of (30, 40) keV with a value of 39°. These energy pairs were further studied with polychromatic spectral analysis.
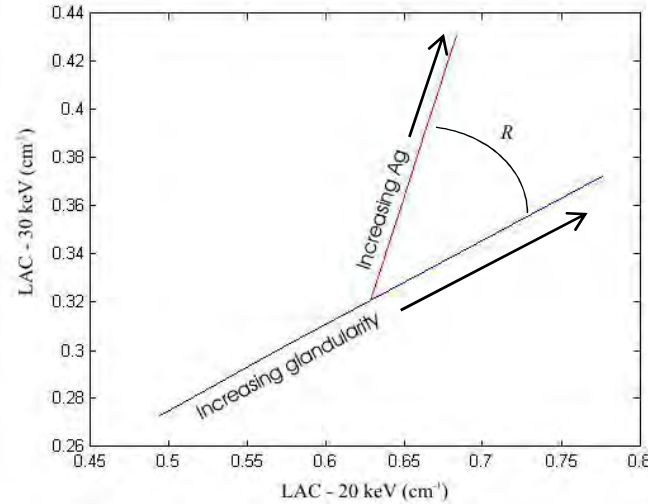

Fig. 1. Two dimensional map of LAC for variations of glandularity and concentration of silver, the metric R was defined as the angle between the two linear fits
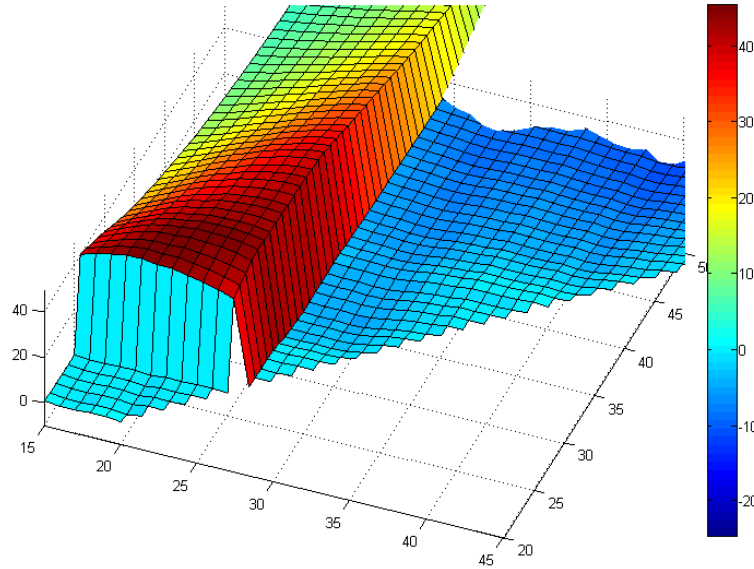
Fig. 2. Surface plot of *R* for various combinations of low- and high- energy pairs. A maximum occurs at (20, 30) keV providing an *R* of 44°

Polychromatic Spectra: Tungsten polychromatic spectra were designed using the interpolating method of Boone et al [2]. Hundreds of combinations of kVp and filter materials were tested until three spectra with mean energies of roughly 20 (S1), 30 (S2) and 40 keV (S3) were chosen, as shown in Table 1. It is expected that a spectral pair of S1, S2 would be more beneficial to a silver contrast agent compared to iodine while a spectral pair of S2, S3 would be better suited to an iodinated contrast agent.

	kVp	Filter Combination	Average Energy (keV)
S1	32	80 μm Ag	21.6
S2	45	0.2 cm Al	30.0
S3	49	0.03 cm Cu	38.0

Table 1. Parameters used for the simulation of the 3 spectra with various average energies. Abbreviations used for the filter: Ag (silver), Al (aluminum), Cu (copper)

Weighting Factors: For each spectrum, the transmission through 1 cm of tissue of varying breast tissue composition (0% to 100 % glandular) was calculated. A thickness of 1 cm was chosen as an initial starting point for our calculations. The transmission was then converted to signal intensity (*S*) given by:

$$S = ln \left(\sum_{E=0}^{kVp} E \times I_E \times e^{-\mu_E t} \right) \quad (1)$$

Where E is the energy in keV, I_E is the incident photon fluence (photons/mm^2) at that energy, μ_E is the linear attenuation coefficient of the breast tissue composition at that energy E, and t is the thickness of tissue. This formulation assumes that an ideal energy-integrating detector is used. The dual-energy signal (S_D) was defined as the weighted subtraction of the low- and high-energy SI:

$$S_D = S_{HE} - w \times S_{LE} \quad (2)$$

For a given pair of tissue glandularities (see Figure 3, G1 and G2), a weighting factor was determined such that the DE signal from G1 was equal to that of G2.

$$S_D(G1) = S_D(G2) \rightarrow w = \frac{H1 - H2}{L1 - L2} \quad (3)$$

Thus, in a DE image no contrast would be observed between these two tissue types using this calculated weighting factor.
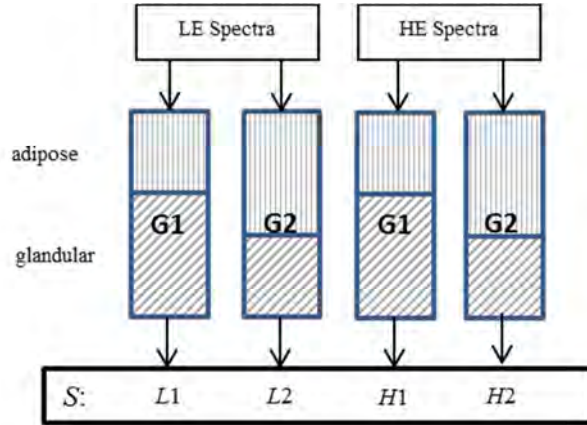

Fig. 3. Schematic setup for determining the weighting factor for a given pair of tissue glandularities (G1, G2). A weighting factor is chosen so as to equate the S_D of the two materials. S_D is given by a weighted subtraction of the high and low signal intensities.

The weighting factor needed to suppress various combinations of tissue glandularities are shown for a high/low spectral combination of S0, S1 (Figure 4) and S1, S2 (Figure 5). The weighting factor is relatively invariant with tissue composition. This would imply that for a given spectral pair of low- and high-energy beams, it should be possible to effectively null the contrast between the underlying tissue structures in the breast.
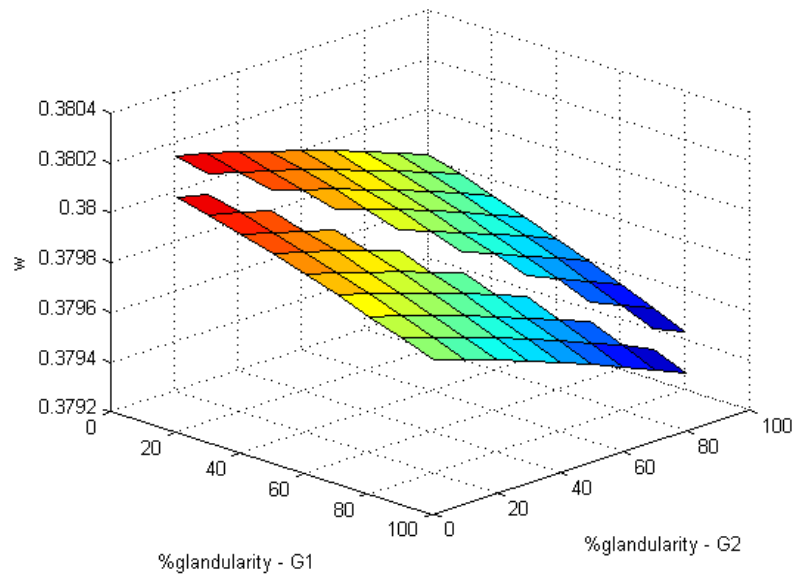
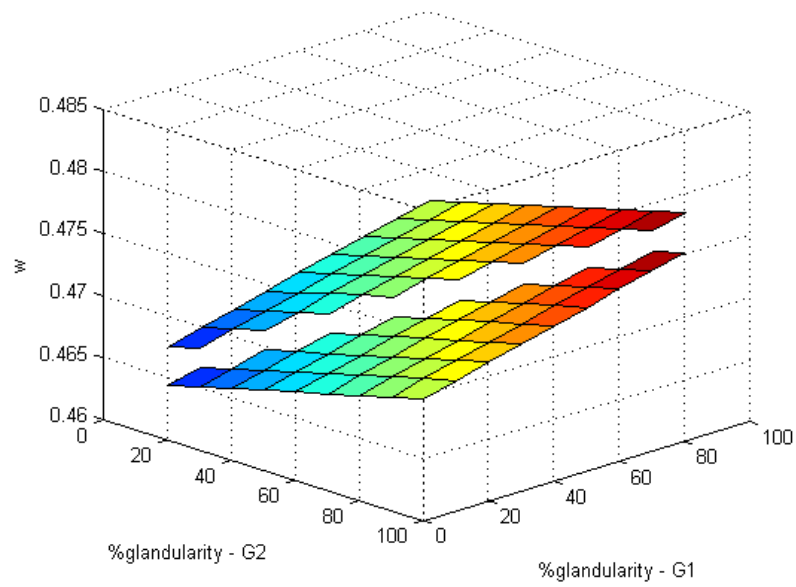**Fig. 4.** Weighting factors calculated for S1 (low) and S2 (high)

Fig. 5. Weighting factors calculated for S2 (low) and S3 (high)

Contrast Calculation: The calculated values of *w* were used to determine DE signals for background tissue (50% adipose, 50 % glandular) and contrast enhanced tissue (50% adipose, 50% glandular + 1mg/mL of contrast material). The contrast (*C*) was calculated as the difference in S_D of tissue with and without contrast material. Values of *C* using silver, iodine and various low/high spectral pairs are tabulated in Table 2. The data correlates well with those predicted by monoenergetic calculations.

1. The contrast observed for each contrast material is greater when using the spectral pair that brackets the k-edge of that material. The contrast observed for silver is greater when using the (S1,S2) spectral pair. Conversely, the contrast observed for iodine is greater when using the (S2,S3) spectral pair.
2. The maximum contrast observed for silver is greater than that of iodine. By comparing the spectral pairs that best suited each material, it was found that the contrast observed for silver was roughly twice that of iodine.

Although these results are not conclusive, they do support our initial hypothesis that silver demonstrates significant potential as a contrast material for dual-energy breast x-ray imaging.

	Spectral Combinations	
C (Digital Units)	**Low E**: S_1 **High E**: S_2	**Low E**: S_2 **High E**: S_3
Silver	20.8 ± 0.003	7.44 ± 0.08
Iodine	9.88 ± 0.004	11.70 ± 0.05

Table 2. Signal Differences tabulated for silver and iodine using various low- and high – energy spectral combinations.

3   Results (Nanoparticle development):

Silver nanoparticles (AgNP) have been synthesized using the Brust [3] method in water. This is preferred over the Turkevich method as it provided a more reliable size distribution of particles from batch to batch. Figure 6 shows a transmission electron micrograph (TEM) of the synthesized particles. Analysis of the size distribution yielded a mean diameter of 4 ±2 nm. Initial analysis showed two populations of nanoparticles present which accounts for the high standard deviation in mean diameter. The AgNP were surface stabilized using polyethylene glycol (PEG, M_w = 5000) to improve solubility in cell media and phosphate buffered solutions. A molar ratio of 1.5:1 was used between the PEG stabilizing ligand and silver.

The cellular toxicity of the stabilized AgNP was measured in T6-17 fibroblast cells using the MTT assay. Figure 7 shows the relationship between concentration of Ag in AgNP and percent cell viability after 24 hour incubation. Compared to a sham treated control, total cell viability of 50% was maintained at an Ag concentration of 10 mM (roughly 1 mg Ag/mL). These results show marked improvement over cell viability studies using AgNP in the literature [4-5] and have encouraged us to begin analysis of the particles in living systems.
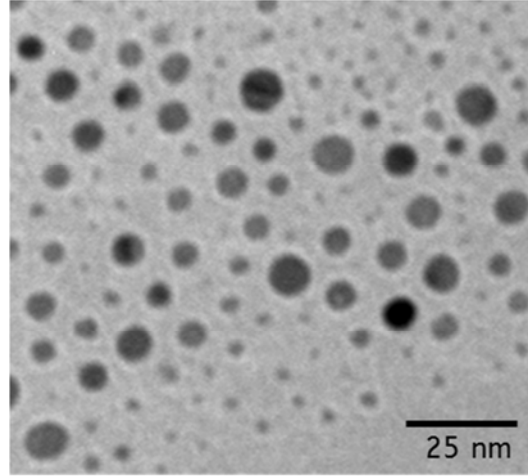
Fig. 6. TEM of the colloidal silver nanoparticles synthesized using the Brust method in water. The particles have been stabilized using a polyethylene glycol surface chain.
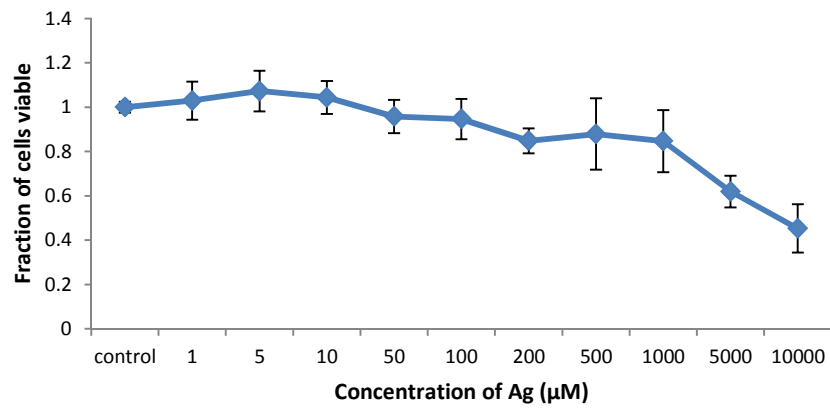

Fig. 7. Cellular toxicity of AgNP in T6-17 cells after 24-hour incubation.

4   Discussion:

Silver is being investigated as a novel imaging agent for dual-energy breast x-ray imaging. Monoenergetic analysis of linear attenuation coefficients showed that compared to iodine it is possible to achieve a greater separation between tissue with and without contrast when silver is used. These results were corroborated by polyenergetic spectra simulation where silver showed up to twice the radiographic contrast of iodine.

It should be noted that only a small subset of the possible spectral pairs were tested in the polyenergetic simulations. The results should therefore not be considered as conclusive as the true optimal contrast values for each material may differ slightly if a more extensive search was performed. However, both the monoenergetic and poly-energetic simulations demonstrate that there exists enormous potential for the use of silver in DE breast x-ray imaging.

Initial work has been completed on the synthesis and testing of AgNP. Spherical AgNP (d = 4 ±2 nm) were synthesized using the Brust method, and stabilized with PEG surface ligands. Little cellular toxicity was observed in cells for silver concentrations up to 1mg/mL. The testing of these particles in living systems is currently underway.

Silver nanoparticles represent an exciting avenue for the development of a novel DE breast x-ray imaging agent. Simulations have demonstrated that within the mammographic energy range, silver is able to offer comparable, if not greater DE contrast to iodine. This work provides the initial groundwork for a rich, new direction in contrast-enhanced DE breast imaging.

Acknowledgements

References

1. National Institute of Standards and Technology (NIST) Physical Measurement Laboratory. *XCOM: Photon Cross Sections Database*. Retrieved December 10, 2011
2. Boone J.M. , Fewell, T.R., Jennings, R.J. Molybdenum, rhodium, and tungsten anode spectral models using interpolating polynomials with application to mammography. Med Phys, 24;12 (1997) 1863 – 1874
3. Brust M., Walker M., Bethell D., Schiffrin D.J., Whyman R., *Synthesis of thiol derivatized gold nanoparticles in a 2-phase liquid-liquid system*. J. Chem. Soc. Chem. Commun. (1994) 801–802.
4. Hussain S., Hess K.L., Gearhart J.M., Geiss K.T., Schlager J.J *In Vitro Toxicity of nanoparticles in BRL 3A rat liver cells*. Toxiciology in Vitro (2005) 975 – 983
5. Navarro E., Piccapietra F., Wagner B., Marconi F., Kaegi R., Odzak N., Sigg L., Behra R. *Toxicity of Silver Nanoparticles to Chlamydomonas reinhardtii* Environmental Science and Technology (2008) 8959 - 89644

Quantification of a silver contrast agent in
dual-energy breast x-ray imaging

Roshan Karunamuni, Andrew D.A. Maidment

Department of Radiology, University of Pennsylvania, Philadelphia, PA 19104

ABSTRACT

Dual-energy (DE) breast x-ray imaging involves acquiring images using a low- and high-energy x-ray spectral pair. These images are then subtracted with a weighting factor that eliminates the soft-tissue signal variation present in the breast leaving only contrast that is attributed to an exogenous imaging agent. We have previously demonstrated the potential for silver (Ag) as a contrast material for DE breast imaging. Theoretical analysis shows that silver can provide better contrast to clinically-used iodine. Here, we present the subtraction method developed to eliminate the contrast between adipose and glandular tissue; the two major component materials in the breast. The weighting factor is calculated from the attenuation coefficients of the two tissue types and varies between values of 0 and 1 for the energy combinations studied. A spectral search was performed to identify the set of clinically-feasible imaging parameters that will optimize the contrast of silver using our subtraction technique. The subtraction methodology was tested experimentally using step-phantoms and demonstrated that we are able to a) nullify the soft-tissue contrast that arises from differences in glandularity, and b) preserve an image contrast for silver that is independent of the underlying soft-tissue composition. By applying the DE subtraction proposed, a silver-based agent will outperform an iodinated contrast agent on a commercially-available CEDE breast x-ray imaging system.

Keywords: breast cancer imaging, dual-energy subtraction, contrast agents, silver

1. INTRODUCTION

Contrast-enhanced dual-energy (CEDE) breast x-ray imaging encompasses an emerging group of modalities that aim to provide quantitative functional information together with high-resolution anatomical data. The unique combination of information in a single imaging procedure represents a powerful breast imaging tool for morphological and vascular characterization of breast lesions [1-4]. DE imaging is used to increase the contrast of radiographic imaging agents by suppressing the anatomical signal variation in the body. In the breast, this involves the suppression of the signal variation that arises from differences in soft tissue (adipose and glandular) composition across the image. By reducing the effect of this soft tissue noise, it is then possible to segment and quantify the signal from an exogenous imaging agent. In CEDE imaging, two distinct energy windows (low- and high-) are used to quantify the variation in attenuation with energy. By employing a contrast agent whose linear attenuation k-edge lies within the energy ranges used, it is possible to separate its signal from the surrounding tissue.

Traditionally, CEDE breast imaging has been employed with an iodinated contrast agent. These agents do, however, possess several limitations that have fueled the research for improved imaging agents [5]. The non-specific nature of the contrast agent results in random vascular permeation, and their relatively low molecular weight facilitates rapid renal clearance. Because these agents lack an appropriate layer of surface biomolecules to prevent the non-specific binding of blood serum proteins, the percentage of the injected dose that reaches the tumor site is low. Perhaps most importantly, iodinated contrast agents were designed for radiographic imaging procedures at much higher x-ray energy ranges than those used in breast imaging. Thus, a more radiographically-suited breast imaging agent is proposed.

We have previously demonstrated the potential for silver as a contrast material for DE breast imaging. Silver represents an attractive base material due to the central location of its k-edge (25.5 keV [6]) in the mammographic clinical energy range. Silver filtration is commonplace in the clinic today, and should allow us to position spectra on either-side of the k-edge. There already exists a significant amount of literature on the development of silver nanoparticles which can be used in the synthesis of a silver-based imaging agent [7-8]. The purpose of this work is to explore, in detail, the DE subtraction methodology needed to remove soft-tissue contrast while maintaining the signal from a silver imaging agent.

2. METHOD

2.1 Imaging Framework

The signal intensity from either the low- or high- energy image can be expressed in terms of the various attenuation coefficients and corresponding thicknesses of materials present in the beam path. In the simplistic case of a monoenergetic x-ray source, these signal intensities can be formulated using the Beer-Lambert law as:

$$\ln(I) = \ln(I_0) + (-\sum \mu t), \tag{1}$$

where I_0 is the initial photon fluence, μ is the linear attenuation coefficient, t is the thickness of the material. In the case of dual-energy breast x-ray imaging, the principal materials that contribute to the attenuation of the x-ray photons are adipose (a), glandular (g) and contrast agent (c). Thus Equation 1, can be rewritten with these three materials for both low-(L) and high-(H) energy photons.

$$\ln(I^L) = \ln(I_0^L) + (-\mu_a^L t_a - \mu_g^L t_g - \mu_c^L t_c) \tag{2}$$

$$\ln(I^H) = \ln(I_0^H) + (-\mu_a^H t_a - \mu_g^H t_g - \mu_c^H t_c). \tag{3}$$

If we then assume that the total thickness of tissue, t can be expressed as the sum of adipose and glandular thicknesses:

$$t = t_a + t_g, \tag{4}$$

we can substitute out t_a in Equations 2 and 3. Thus the signal intensity at each energy level can be described in terms of the total thickness of tissue, the amount of glandular tissue, and the amount of contrast material:

$$\ln(I^L) = \ln(I_0^L) - \mu_a^L t + t_g(\mu_a^L - \mu_g^L) - \mu_c^L t_c \tag{5}$$

$$\ln(I^H) = \ln(I_0^H) - \mu_a^H t + t_g(\mu_a^H - \mu_g^H) - \mu_c^H t_c \tag{6}$$

The DE signal intensity (SI_{DE}) can be expressed as a weighted (W) subtraction between the high- and low- energy signal intensities.

$$SI^{DE} = \ln(I_0^H) - W \times \ln(I_0^H) + t \times [-\mu_a^H + W \times \mu_a^L] + t_g \times [(\mu_a^H - \mu_g^H) - W \times (\mu_a^L - \mu_g^L)] + t_c \times [-\mu_c^H + W \times \mu_c^L] \tag{7}$$

SI^{DE} can be broken down into three major components. The first component, $\ln(I_0^H) - W \times \ln(I_0^H) + t \times [-\mu_a^H + W \times \mu_a^L]$, is a combination of the initial photon fluence and total thickness of the breast. This component can be assumed to be constant across the image and thus provides an offset to SI^{DE}. The second component, $t_g \times [(\mu_a^H - \mu_g^H) - W \times (\mu_a^L - \mu_g^L)]$, describes the relationship between SI^{DE} and the amount of glandular tissue in the beam. By choosing W as:

$$W = \frac{\mu_a^H - \mu_g^H}{\mu_a^L - \mu_g^L}, \tag{8}$$

we can eliminate this dependence. Thus the only remaining term that varies across the image is the third component $t_c[-\mu_c^H + w \times \mu_c^L]$. This component quantifies the linear relationship between SI^{DE} and the thickness of contrast material The contrast, S_C, can be defined as the change in SI_{DE} with respect to t_c :

$$\frac{d(SI^{DE})}{d(t)} = S_C = -\mu_c^H + \frac{\mu_a^H - \mu_g^H}{\mu_a^L - \mu_g^L} \times \mu_c^L, \tag{9}$$

2.2 Monoenergetic Simulation Testing

The subtraction method was tested using a computer-simulated, monoenergetic x-ray acquisition. Photons of a single energy are passed through a 5 cm step-wedge phantom that consists of sections ranging from 0 to 100% glandular, in 25% increments. The photons are then recorded on an ideal, energy-integrating detector in the absence of scatter or glare. A section of the phantom is replaced with breast material that has been mixed with a certain

concentration of silver. In this manner, simulated high- and low- energy images were acquired and then subtracted using the weighting factors calculated in (8).

2.3 Spectral Optimization

A spectral simulation search was performed to identify the combination of clinically-feasible imaging parameters that maximized contrast for Ag. The parameters chosen for the search are limited to those that are experimentally feasible on the Hologic CEDE Dimensions system.

Table 1. Parameters used for the spectral search.

Parameter	Values
Target	Tungsten
Low Energy kVp	23 to 32
High Energy kVp	36 to 49
Filter Materials	**Low Energy**: Ag, Rh, Al
	High Energy: Cu
	All spectra were pre-filtered with 50 cm of air and 0.7 mm Be
Detector	Si, energy-integrating

Polyenergetic tungsten spectra were simulated using Boone's interpolation method and filtered using the Beer-Lambert law. The signal intensity recorded on the detector was calculated as:

$$SI = \sum_{E=1}^{kVp} N_E \times F_m \times F_d \times E \tag{10}$$

where:

N_E is the number of photons at the energy E, calculated using Boone's method [9].
$F_m = e^{\Sigma(-\mu t)}$ for all materials present in the beam path
$F_d = (1 - e^{-(\mu t)_d})$ for the detector (d)

The standard deviation, σ, of the signal intensity was calculated as:

$$S\sigma = SI^{0.46} \tag{11}$$

The coefficient of 0.46 was obtained from Marshall *et al.* where the noise in a Hologic Selenia system was characterized. A low- and high- energy spectral pair were then passed through either a block of 100% adipose or 100% glandular tissue. *W* can be calculated using signal intensities (SI) as:

$$W = \frac{\ln(SI_a^H) - \ln(SI_g^H)}{\ln(SI_a^L) - \ln(SI_g^L)} \tag{12}$$

Equation 12 can be thought of as the equivalent of Equation 8 for a polyenergetic spectra. The spectral pair used for the calculation of *W* was then instead passed through a block with a 50% glandular fraction. SI^{DE} was calculated in the presence (SI_{Ag}^{DE}) and absence (SI_{bkg}^{DE}) of a silver contrast agent at a concentration of 1 mg/cm². The signal difference to noise ratio (SDNR) was chosen as the figure of merit to be maximized in the optimization, and was calculated as:

$$SDNR = \frac{SI_{Ag}^{DE} - SI_{bkg}^{DE}}{\sigma_{bkg}^{DE}} \tag{13}$$

where:

$$\sigma^{DE} = \sqrt{\sigma^{2H} + W^2 \times \sigma^{2L} - 2 \times W \times cov(\ln(SI_{bkg}^H), \ln(SI_{bkg}^L))} \tag{14}$$

The covariance term was assumed to be a constant and determined experimentally by obtaining a DE image set of a plain sheet of acrylic, and then calculating the correlation between the signals in a fixed region of interest.

To ensure that the results would produce an optimization point that was clinically feasible, several constraints were applied to the simulation algorithm:

- The total effective dose to the breast was set at 2.4 mGy. However, the manner in which this dose was distributed between the low- and high- energy spectra was allowed to vary. The mean glandular dose to the breast for a given spectrum was calculated using Hendee [10] and Dance [11].

- The mAs required to achieve the desired dose was not allowed to exceed 200 mAs. The required mAs for a given dose was estimated using experimentally-obtained tube output data.

- A minimum threshold detector signal intensity was set.

2.4 Spectral Optimization Validation

A 4cm step phantom was imaged on the Hologic clinical CEDE Dimensions system. A silver foil, measuring 50 µm in thickness, was taped on top of the phantom to mimic an embedded concentration of 25 mg/cm^2 of Ag contrast agent. The phantom was imaged at the optimal conditions found in the previous section as well as other non-optimal combinations of parameters. The low- and high- energy images were then subtracted using the appropriate weighting factors to eliminate the glandular dependence. *SDNR* was then calculated for each of the DE images. The experimental and simulated values of W and SDNR were compared to validate the simulation algorithm.

3. RESULTS

3.1 Imaging Framework

W (see Figure 1) and S_C of silver (see Figure 2) were calculated for energy combinations between 20 and 50 keV. W was found to have values ranging between 0 and 1 – this is to be expected as the difference in mass attenuation coefficients of adipose and glandular tissue decreases as the energy increases. W tends towards 1 along the diagonal of the plot, for the case where the low and high energy are equal, and is smallest when the low- and high- energies are furthest apart.
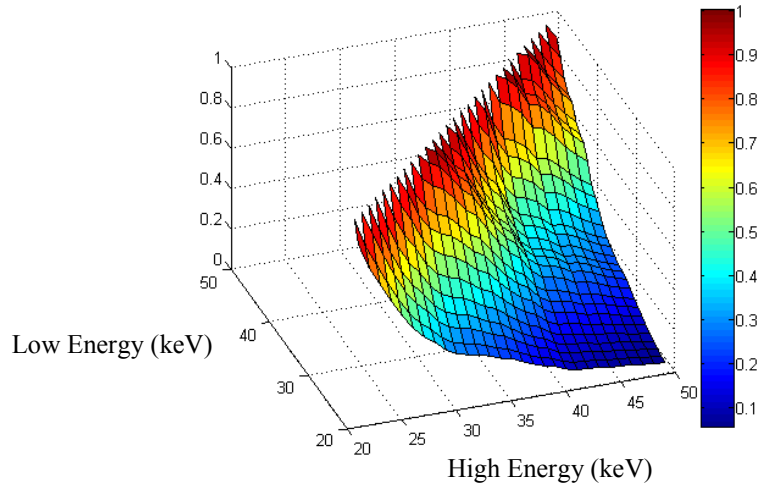

Figure 1. W calculated for energy combinations ranging from 20 to 50 keV. Values ranged from 0 to 1.

As expected, S_C is only significantly greater than zero for energy pairs that bracket the k-edge. The maximum contrast, however, does not occur directly above and below the k-edge but at (21,26) keV. This is due to the effect that the weighting factor, and consequently the attenuation coefficients of adipose and glandular tissue, have on S_C.

Similarly, S_C was calculated for iodine, and plotted in Figure 3. The maximum achievable contrast when using iodine is 33% lower than that of silver.
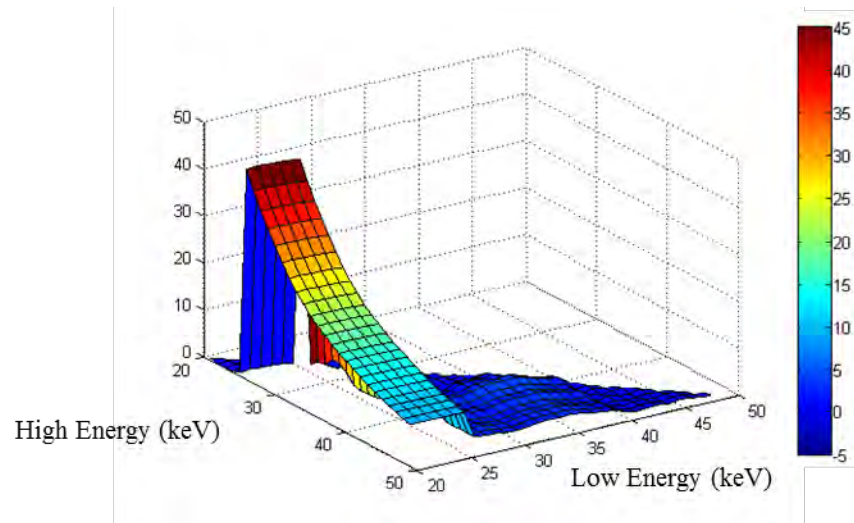

Figure 2. S_C calculated for silver at energy pairs between 20 and 50 keV. The maximum contrast of 45 a.u. occurs at a low energy of 21 keV, and a high energy of 26 keV.
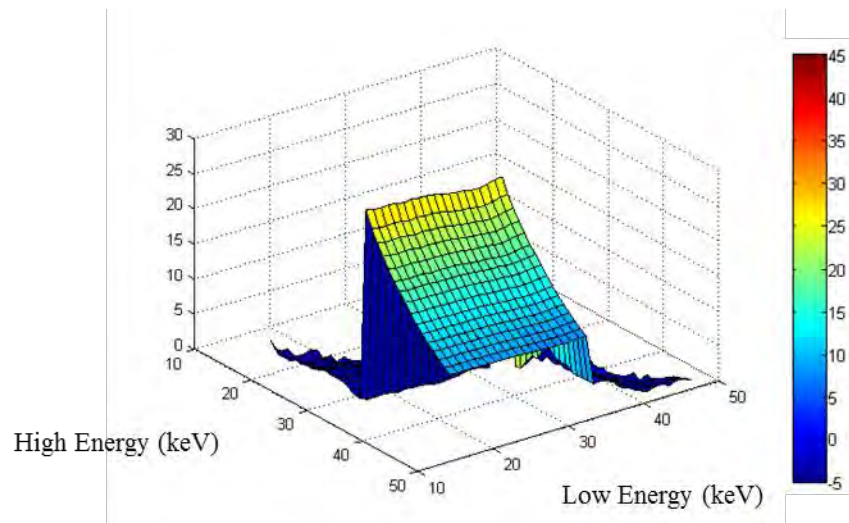

Figure 3. S_C calculated for iodine at energy pairs between 15 and 50 keV. The maximum achievable contrast is 33% lower than that of silver.

3.2 Monoenergetic Simulations

Figure 4 shows the simulated low- and high- energy images that are obtained using an energy pair of (21,26) keV. Each of the single energy images demonstrates a strong SI-dependence on the glandular fraction of the underlying tissue. The section of the phantom that contains Ag, consists of a singular concentration of the element, but results in a gradient of signal intensities because of the underlying variations in soft-tissue composition. By subtracting these single-energy images using W calculated for that energy pair, the DE image shown on the right was obtained.
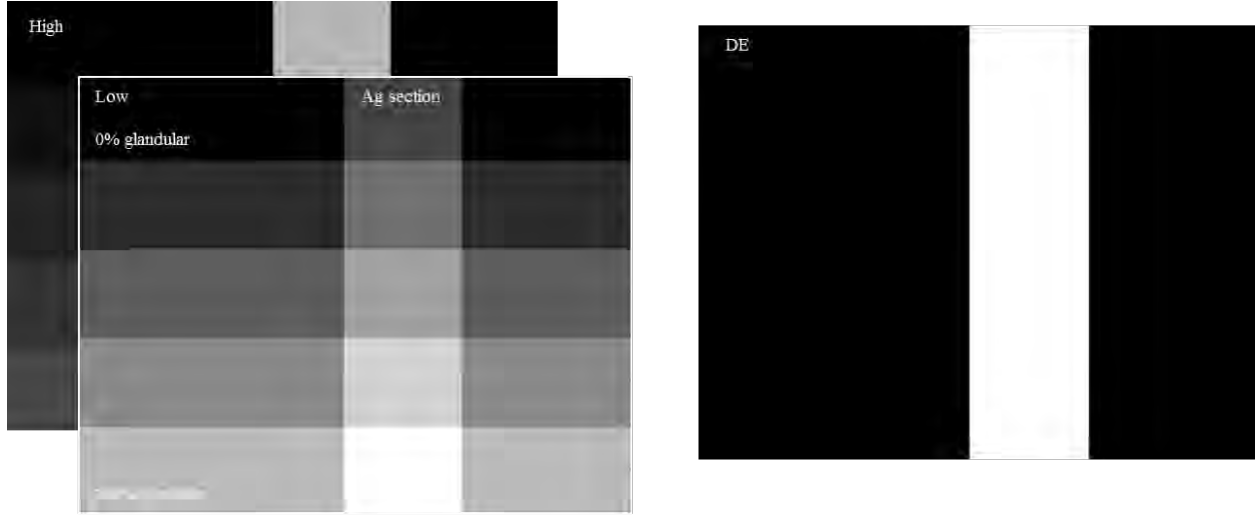
Figure 4. High (26 keV)- and Low (21 keV)- energy images of a step phantom with an section of embedded Ag. The images are subtracted using the pre-calculated weighting factor to yield the DE image shown on the right.

3.3 Spectral Optimization and Validation

Five spectral pairs, including the optimization maximum, were chosen to validate the simulation results (see Table 2). Figure 5 shows the experimentally-determined *W* plotted against the simulated values. The two sets of data are shown to be highly correlated, with the experimental values assuming a scalar multiple of the simulated data. This scalar is due to the manner in which the Hologic CEDE converts the total number of x-ray photons into digital values.

The *SDNR* simulated for each of these spectra was compared to the experimentally-obtained values and plotted in Figure 6. The two sets of data are found to be correlated with a coefficient of determination, R^2, of 0.9407. Spectral Pair 1 was identified as the optimization maximum in the simulation algorithm, and also showed the maximum experimental *SDNR*. An identical simulation algorithm was run for an iodine contrast agent, and the maximum *SDNR* was calculated to be 15% lower than that of Spectral Pair 1.

Low- and high-energy images, along with the DE subtraction, are shown in Figure 7 for the step phantom imaged using Spectral Pair 1. A line segment (shown in blue), spanning all glandular fractions, was placed in each of the DE, low-, and high-energy images. The mean (γ) and standard deviation (σ) of the SI of the pixels in a given image were then calculated, and the coefficient of variation c_v of the background SI was computed as:

$$c_v = \frac{\gamma}{\sigma} \tag{15}$$

Similarly, six square regions of interest (Figure 7, 5 in red over the silver, 1 in green over the background) were used to calculate the SDNR at five locations of the phantom marked with red squares. c_v of the SDNR and background SI are tabulated in Table 3. In each case, c_v is smallest in the DE image.

Table 2. Spectra chosen for validation of optimization results. The table includes the high- and low- energy kVp and filter choice along with the dose fraction to the low-energy spectrum. The optimization maximum is highlighted in gray.

Spectral Pair	High Energy	Low Energy	Dose fraction to LE
1	46 - Cu	27 - Rh	0.5
2	49 - Cu	27 - Al	0.6
3	49 - Cu	34 - Ag	0.6
4	49 - Cu	33 - Rh	0.8
5	40 - Cu	35 - Al	0.8

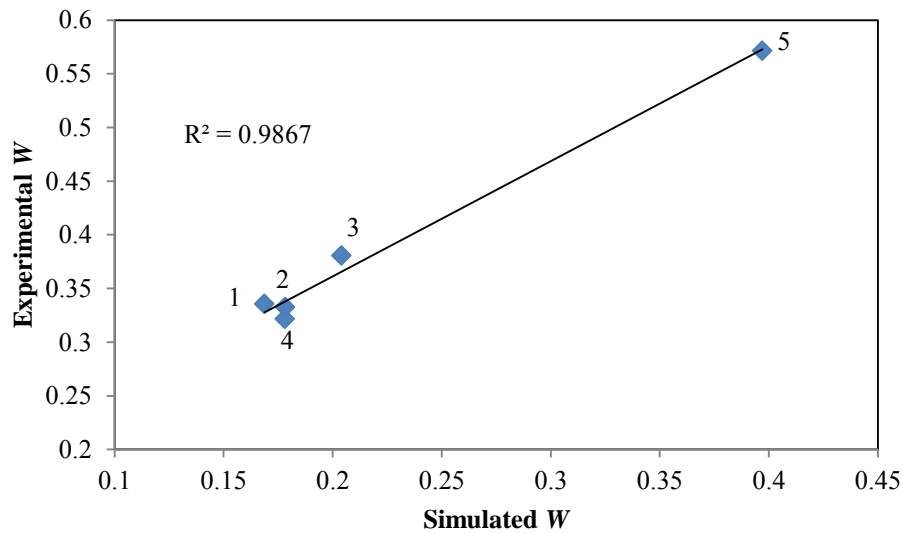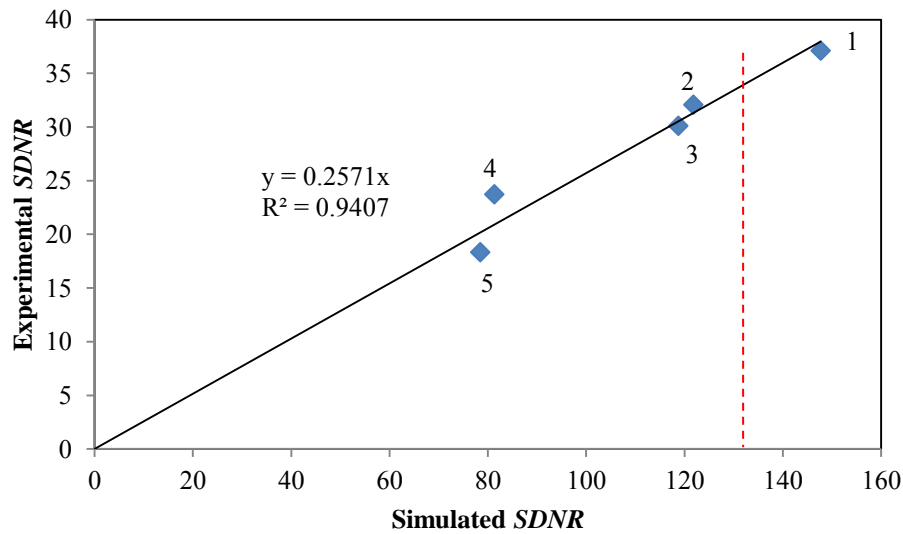**Figure 5.** The experimental and simulated values of *W* show excellent agreement.

Figure 6. Correlation between simulated and experimental *SDNR* values. The data shows excellent agreement between the simulated and experimentally-obtained values, with the optimization point providing the maximum in both. The red dashed line indicates the maximum simulated SDNR for iodine, calculated under the same constraints.
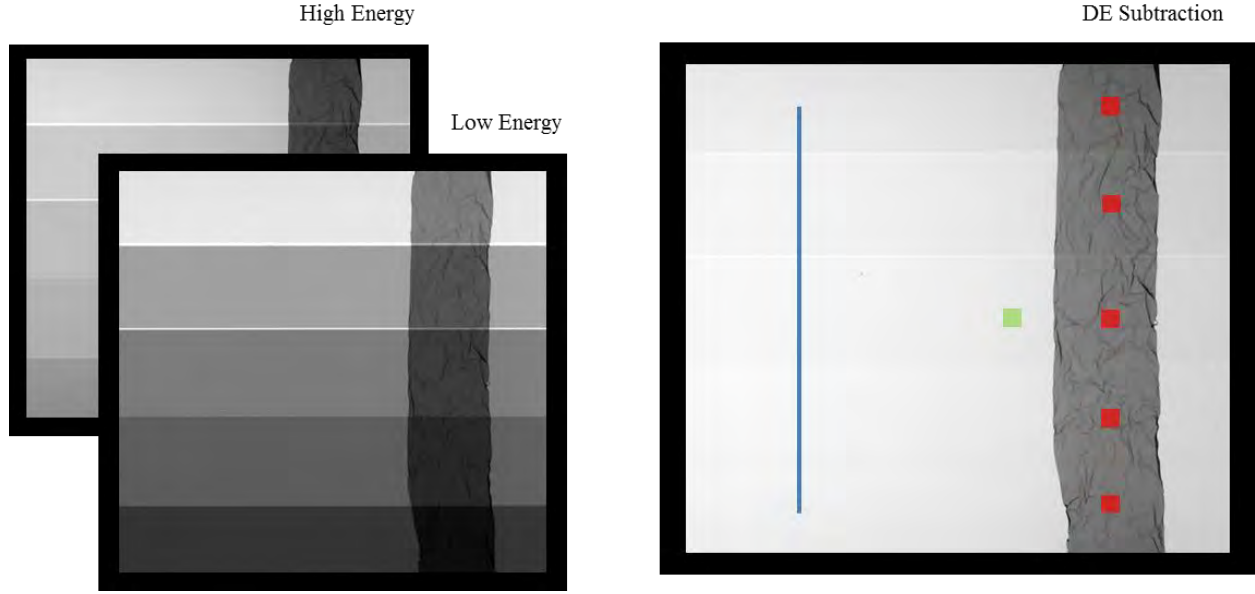
Figure 7. Low- and high-energy images along with the DE subtraction of a 4 cm step phantom with a silver foil emulating an areal concentration of 25 mg/cm^2. The artifacts present in the image of the foil arise from physical imperfections in the material.

Table 3. Coefficient of variation, c_v, for the background SI and SDNR in each of the DE, low- and high-energy images. For both cases, c_v of the DE image is the smallest.

c_v	DE	Low-Energy	High Energy
Background SI	0.072	0.71	0.12
SDNR	0.0036	0.28	0.0095

4. DISCUSSION AND CONCLUSIONS

The goal of this study was to develop a DE subtraction method for silver that would remove soft tissue signal variation while preserving the contrast from the imaging agent. A framework was developed in Equations 1 through 9 using a monoenergetic analysis of the signal intensities obtained from a low- and high-energy acquisition. The weighting factor, W, that is needed to be applied to the low-energy image in the DE subtraction is formulated in Equation 8. W is independent of the choice of contrast material, and solely depends on the low- and high-energy attenuation coefficients of adipose and glandular tissue. W is plotted in Figure 1 for combinations of energies ranging from 20 to 50 keV. W assumes values between 0 (when the low- and high-energies are furthest apart) and 1 (for the trivial case when the low- and high-energy are the same).

The theoretical DE contrast, S_C, observed from an imaging agent is formulated in Equation 9. S_C is plotted in Figures 2 and 3 for silver and iodine, respectively. For both materials, S_C is only significantly greater than zero at energy pairs that bracket the k-edge of the material (25 keV – silver, 33 keV – iodine). Interestingly, the maximum value of S_C does not occur directly above and below the k-edge where the difference between the attenuation coefficient is the greatest. Instead, S_C of silver is maximum at an energy pair of (LE,HE) = (21,26) keV. This is due to the effect that the weighting factor, and consequently the attenuation coefficients of adipose and glandular tissue, have on S_C. The maximum achievable contrast of iodine is 33% lower than that of silver, implying that a silver contrast agent would be better suited as a DE imaging agent in the mammographic energy range.

A monoenergetic image acquisition was then simulated using the energy pair (21, 26) keV that maximized S_C of silver. Figure 4 shows the DE, low-,and high-energy images that were obtained. The DE image demonstrates two important features that are critical to CEDE imaging. First, the soft-tissue contrast has been nullified. The

background signal has been reduced to a single value that is independent of the glandular percentage. Second, the contrast in the silver is maintained and independent of the underlying soft-tissue composition

A polyenergetic simulation was then performed to identify the set of clinically-feasible imaging parameters that optimized the contrast for silver. In this particular study, the optimization was performed for a Hologic CE-DBT system; parameters listed in Table 1. The simulation was further constrained to ensure that the total mean glandular dose to the breast was 2.4 mGy. The optimal imaging technique consisted of a 46 kVp high-energy beam and a 27 kVp low-energy beam with rhodium filtration, at a dose distribution of 50:50. This low-energy technique is a classic example of an anatomical image that is obtained in the clinic today. In the case of an iodine agent, this low-energy kVp would need to be higher to accommodate for the higher k-edge of iodine. This further supports our hypothesis that silver is a superior DE imaging agent to iodine in the mammographic energy range.

Table 2 shows the four additional spectral pairs that were chosen to test the validity of the simulation algorithm identifying Spectral Pair 1 as the optimization point. The experimental values of W for each of the spectral pairs was shown to correlate well with the simulated numbers as shown in Figure 5. The inability to perfectly estimate W arises from the inability to exactly simulate the conversion of x-ray photons absorbed in the detector to digital units. As shown in Figure 6, the experimentally-determined SDNR was shown to highly correlated with the simulated values . Spectral Pair 1 proved to maximize the SDNR in both the experiments and simulations. Additionally, the maximum simulated SDNR for an iodine agent is 15% lower than that of Spectral Pair 1, further supporting that silver is a better DE imaging agent in the mammographic energy range.

DE, low-, and high-energy images of the step phantom imaged using Spectral Pair 1 is shown in Figure 7. The coefficient of variation, c_v, of the background SI and the SDNR of the silver at various locations in the phantom are tabulated in Table 3. In both cases, the DE image demonstrates the lowest c_v. This indicates that the DE subtraction succeeded in removing the soft-tissue signal variation present at the single-energy images, as well as maintaining the SDNR of a silver contrast agent regardless of the underlying soft-tissue composition. This work leads us to believe that by applying the DE subtraction proposed, a silver-based agent will outperform an iodinated contrast agent on a commercially-available CEDE breast x-ray imaging system.

5. REFERNCES

1. Carton AK, Ullberg C, Lindman K, Acciavati R, Francke T, Maidmenet ADA. Optimization of a dual-energy contrast-enhanced technique for a photon-counting digital breast tomosynthesis system: I. A theoretical model. Med Phys. 2010 Nov; 37(11): 5896 -5907
2. Carton AK, Ullberg C, Maidment ADA. Optimization of a dual-energy contrast-enhanced technique for a photon-counting digital breast tomosynthesis system: II. An experimental validation. Med Phys. 2010 Nov; 37(11):5908-5913
3. Carton AK, Gavenonis S, Currivan JA, Conant E, Schnall MD, Maidment ADA. Dual-energy contrast-enhanced digital breast tomosynthesis – a feasibility study. British Journal of Radiology. 2010; 83:344-350
4. Chen SC, Carton AK, Albert M, Conant E, Schnall MD, Maidment ADA. Initial clinical experience with contrast-enhanced digital breast tomosynthesis. Acad Radiol. 2007 Feb; 14(2):229-238
5. Hainfeld J, Slatkin DN, Focella TM, Smilowitz HM. Gold particles: a new X-ray contrast agent. British Journal of Radiology. 2006 Mar; 79:248-253
6. NIST.gov [homepage on the Internet]. NIST X-ray Transition Energies; 2011 [updated 2011 December 9; cited 2013 Feb 19]. Available from: http://www.nist.gov/pml/data/xraytrans/index.cfm
7. Sun Y, Xia Y. Shape-Controlled Synthesis of Gold and Silver Nanoparticles. Science. 2002 Dec 13; 298: 2176-2179
8. Wang Y, Zheng Y, Huang CZ, Xia Y. Synthesis of Ag Nanocubes 18 – 32 nm in Edge Length: The Effects of Polyol on Reduction Kinetics, Size Control, and Reproducibility. JACS. 2013 Jan 14; 135:1941-1951
9. Boone JM, Fewell TR, Jennings R. Molybdenum, rhodium, and tungsten anode spectral models using interpolating polynomials with application to mammography. Med Phys. 1997 Dec; 24(12):1863-1874
10. Hendee WR, Ritenour ER. Medical Imaging Physics. 4th ed. Wiley-Liss (NY); 2002.
11. Dance DR. Monte Carlo calculation of conversion factors for the estimation of mean glandular breast dose. Phys Med Biol. 1990; 35(9):1211-1219